Energy Budgets on the Interactions between the Mean and Eddy Flows during a Persistent Heavy Rainfall Event over the Yangtze River Valley in Summer 2010

FU Shenming[1*] (傅慎明), WANG Huijie[2] (汪汇洁), SUN Jianhua[3] (孙建华), and ZHANG Yuanchun[3] (张元春)

1 *International Center for Climate and Environment Sciences, Institute of Atmospheric Physics,*
Chinese Academy of Sciences, Beijing 100029

2 *Beijing Institute of Aeronautical Meteorology, Beijing* 100085

3 *Laboratory of Cloud-Precipitation Physics and Severe Storms, Institute of Atmospheric Physics,*
Chinese Academy of Sciences, Beijing 100029

ABSTRACT

In this study, a persistent heavy rainfall event (PHRE) that lasted for around 9 days (from 0000 UTC 17 to 0000 UTC 26 June 2010) and caused accumulated precipitation above 600 mm over the Yangtze River valley, was reasonably reproduced by the advanced research WRF model. Based on the simulation, a set of energy budget equations that divided the real meteorological field into the mean and eddy flows were calculated so as to understand the interactions between the precipitation-related eddy flows and their background circulations (BCs). The results indicated that the precipitation-related eddy flows interacted with their BCs intensely during the PHRE. At different layers, the energy cycles showed distinct characteristics. In the upper troposphere, downscaled energy cascade processes appeared, which favored the maintenance of upper-level eddy flows; whereas, a baroclinic energy conversion, which reduced the upper-level jet, also occurred. In the middle troposphere, significant upscaled energy cascade processes, which reflect the eddy flows' reactionary effects on their BCs, appeared. These effects cannot be ignored with respect to the BCs' evolution, and the reactionary effects were stronger in the dynamical field than in the thermodynamical field. In the lower troposphere, a long-lived quasi-stationary lower-level shear line was the direct trigger for the PHRE. The corresponding eddy flows were sustained mainly through the baroclinic energy conversion associated with convection activities. Alongside this, the downscaled energy cascade processes of kinetic energy, which reflect the direct influences of BCs on the precipitation-related eddy flows, were also favorable. A downscaled energy cascade of exergy also appeared in the lower troposphere, which favored the precipitation-related eddy flow indirectly via the baroclinic energy conversion.

Key words: persistent heavy rainfall, kinetic energy, available potential energy, scale interaction, Yangtze and Huaihe River valley

1. Introduction

Persistent heavy rainfall events (PHREs) have long been a focus of study in China, due to their ability to trigger flash floods, debris flow, and urban waterlogging, all of which seriously threaten people's lives and properties (Tao, 1980; Zhao et al., 2004; Zhai et al., 2005; Xia et al., 2006; Xia and Zhao, 2009; Fu et al., 2010; Hou and Guan, 2013; Wang et al., 2014; Zong et al., 2014; Li et al., 2016). For instance, the severe flooding events of the Huaihe River in 1991, 2003, and 2007, and the disastrous flooding events of the Yangtze River in 1998 and 1999, were all triggered directly by PHREs. In recent years, against the background of

global warming, the intensity category of PHREs (which is determined according to the intensity of precipitation) has shown a significant increasing trend, not only in frequency but also in rainfall strength (Wang et al., 2014; Fu et al., 2016; Li et al., 2016), which markedly increases the flooding risk in China. Therefore, special attention should be paid to these destructive events.

For many years, considerable effort has been made to understand PHREs. Tao and Xu (1962) proposed that the quasi-stationary behavior of background circulations (BCs) was a necessary condition for a PHRE. Ding (1994) pointed out that, during PHREs, frequent occurrence of synoptic and/or mesoscale weather systems over the same region can render a considerable amount of accumulated precipitation that may result in severe flooding. Xu et al. (2002) suggested that many PHREs over the middle reaches of the Yangtze River and South China are closely related to the activities of the Madden–Julian Oscillation. Chen and Zhao (2004) found that the South China Sea summer monsoon provides favorable moisture conditions for PHREs over South China. Zhao and Fu (2007) analyzed a long-lived southwest vortex that caused a PHRE in September 2004. They found that the release of available potential energy contributed to the maintenance of the vortex, and the weak steering flow rendered the qusai-stationary behavior of the vortex, which significantly enhanced the accumulated precipitation locally. Yin et al. (2009) reported the climatological features of PHREs over Guizhou Province by conducting a 54-yr statistical analysis. Wang et al. (2014) classified the PHREs over South China during 1981–2011 into five basic types. They concluded that both the occurrence frequency and precipitation intensity of the PHREs showed a significant increasing trend after 2000.

Previous studies have confirmed that multiscale weather systems interact intensely with one another during a PHRE (Tao, 1980; Xia and Zhao, 2009; Fu et al., 2015). This ranges from large-scale systems such as the intertropical convergence zone (Ninomiya and Muraki, 1986), western Pacific subtropical high (Zhao et al., 2004), and East Asian summer monsoon (Ding et al., 2007), to mesoscale and small-scale systems such as the southwest vortex (Fu et al., 2011), mesoscale convective system (Chen et al., 2006), and even Ekman pumping (Cho and Chen, 1995). However, thus far, how large-scale BCs and the direct PHRE triggers (i.e., the synoptic- and subsynoptic-scale weather systems) interact with one another remains an open question. Therefore, the primary purpose of this study is to understand the interactions between the mean flow and the eddy flow (direct precipitation trigger) during a PHRE from the viewpoint of energy.

The remainder of this paper is structured as follows. Section 2 details the model configuration, data, and methodology. Section 3 describes the selected PHRE case. Section 4 reports the main energy budget results. Finally, conclusions are drawn in Section 5.

2. Model configuration, data, and methodology

The advanced research WRF model version 3.4 (Michalakes et al., 2004) was used in this study. The 6-h and $1° \times 1°$ NCEP final (FNL) operational global analysis data were used as the initial and boundary conditions for the simulations. The $0.25° \times 0.25°$ daily OISST (Optimum Interpolation Sea Surface Temperature) dataset (Reynolds et al., 2007) was used for the sea surface temperature conditions. The China Meteorological Administration (CMA) 3-h surface observations and 12-h soundings (available at 0000 and 1200 UTC) were used to improve the first guess of the outer domain through an objective analysis method (Michalakes et al., 2004). The observational data were also used to validate the simulation results. Two domains with two-way nesting were used in this study (Fig. 1). The horizontal resolutions of the outer and inner domains were 81 and 27 km, respectively. There were a total of 37-η levels in the simulations, with the model top fixed at 10 hPa. The YSU (Yonsei University) planetary boundary layer scheme (Hong et al., 2006), Noah land surface model (Chen and Dudhia, 2001), WRF double-moment 6-class microphysics scheme (Lim and Hong, 2010), and Kain-Fritsch cumulus parameterization (Kain, 2004), were used in both

domains.

The eddy kinetic energy (KE) budget equations (Kucharski and Thorpe, 2000) were used in this study to understand the interactions between the PHRE-related eddy flows and their BCs. A concise form of the budget equations is as follows.

$$\frac{\partial(\overline{\rho}k_{\mathrm{m}})}{\partial t} = -\nabla \cdot [\overline{\rho}\langle\boldsymbol{V}\rangle k_{\mathrm{m}} + \langle\boldsymbol{V}\rangle \cdot \overline{\rho\boldsymbol{V}''\boldsymbol{V}''} + \overline{\boldsymbol{F}} \cdot \langle\boldsymbol{V}\rangle] - C(\overline{\rho}k_{\mathrm{m}}, \overline{\rho k_{\mathrm{t}}}) - C(\overline{\rho}k_{\mathrm{m}}, \overline{\rho}e_{\mathrm{m}}) - D(\overline{\rho}k_{\mathrm{m}}),$$

$$\text{MTKM} \qquad \text{RSW} \qquad \text{MSM} \qquad \text{CKMT} \qquad \text{BCM} \qquad \text{MDM}$$
(1)

$$\frac{\partial(\overline{\rho}e_{\mathrm{m}})}{\partial t} = -\nabla \cdot [\overline{\rho}\langle\boldsymbol{V}\rangle e_{\mathrm{m}} + \langle T\rangle\eta_{\mathrm{m}}\frac{c_{\mathrm{p}}}{\langle\theta\rangle} \cdot \overline{\rho\boldsymbol{V}''\theta''} + (\overline{p} - p_{\mathrm{R}})\langle\boldsymbol{V}\rangle] - C(\overline{\rho}e_{\mathrm{m}}, \overline{\rho e_{\mathrm{t}}}) + C(\overline{\rho}k_{\mathrm{m}}, \overline{\rho}e_{\mathrm{m}}) + G(\overline{\rho}e_{\mathrm{m}}),$$

$$\text{MTEM} \qquad \text{ETH} \qquad \text{WMP} \qquad \text{CEMT} \qquad \text{BCM} \qquad \text{GEM}$$
(2)

$$\frac{\partial(\overline{\rho k_{\mathrm{t}}})}{\partial t} = -\nabla \cdot [\overline{\rho\boldsymbol{V}k_{\mathrm{t}}} + \overline{\boldsymbol{F} \cdot \boldsymbol{V}''}] + C(\overline{\rho}k_{\mathrm{m}}, \overline{\rho k_{\mathrm{t}}}) + C(\overline{\rho k_{\mathrm{t}}}, \overline{\rho e_{\mathrm{t}}}) - D(\overline{\rho k_{\mathrm{t}}}),$$

$$\text{TKT} \qquad \text{MSE} \qquad \text{CKMT} \qquad \text{BCE} \qquad \text{MDE}$$
(3)

$$\frac{\partial(\overline{\rho e_{\mathrm{t}}})}{\partial t} = -\nabla \cdot [\overline{\rho\boldsymbol{V}e_{\mathrm{t}}} + \overline{p'\boldsymbol{V}''}] + C(\overline{\rho}e_{\mathrm{m}}, \overline{\rho e_{\mathrm{t}}}) - C(\overline{\rho k_{\mathrm{t}}}, \overline{\rho e_{\mathrm{t}}}) + G(\overline{\rho e_{\mathrm{t}}}),$$

$$\text{TET} \qquad \text{WPP} \qquad \text{CEMT} \qquad \text{BCE} \qquad \text{GET}$$
(4)

where the overbar represents a zonal average of a variable. $\langle\psi\rangle = \dfrac{\overline{\rho\psi}}{\overline{\rho}}$ stands for a density-weighted average of a sample variable ψ, its corresponding perturbation is defined as $\psi'' = \psi - \langle\psi\rangle$; and ρ is the air density. The mean and perturbation KE are $k_{\mathrm{m}} = \frac{1}{2}\langle\boldsymbol{V}\rangle \cdot \langle\boldsymbol{V}\rangle$ and $k_{\mathrm{t}} = \frac{1}{2}\boldsymbol{V}'' \cdot \boldsymbol{V}''$, respectively; e_{m} and e_{t} denote the mean exergy and perturbation exergy, respectively. According to Kucharski and Thorpe (2000), the exergy is a local formulation of the available potential energy. T is the temperature, η_{m} is the mean Carnot factor, c_{p} is the specific heat of dry air at constant pressure, θ is the potential temperature, F is the molecular stress tensor, and the subscript R denotes the reference state. Term $-\nabla \cdot [\overline{\rho}\langle\boldsymbol{V}\rangle k_{\mathrm{m}}]$ represents the mean transport of k_{m} (MTKM); $-\nabla[\langle\boldsymbol{V}\rangle \cdot \overline{\rho\boldsymbol{V}''\boldsymbol{V}''}]$ stands for the Reynolds stress work (RSW) on the mean flow; $-\nabla \cdot [\overline{\boldsymbol{F}} \cdot \langle\boldsymbol{V}\rangle]$ denotes the molecular stress effect on the mean flow (MSM); $C(\overline{\rho}k_{\mathrm{m}}, \overline{\rho k_{\mathrm{t}}})$ is the energy conversion between k_{m} and k_{t} (CKMT); $C(\overline{\rho}k_{\mathrm{m}}, \overline{\rho}e_{\mathrm{m}})$ stands for the baroclinic energy conversion between k_{m} and e_{m} (BCM); $D(\overline{\rho}k_{\mathrm{m}})$ represents the molecular dissipation of k_{m} (MDM); $-\nabla \cdot [\overline{\rho}\langle\boldsymbol{V}\rangle e_{\mathrm{m}}]$ is the mean transport of e_{m} (MTEM); $-\nabla[\langle T\rangle\eta_{\mathrm{m}}\frac{c_{\mathrm{p}}}{\langle\theta\rangle} \cdot \overline{\rho\boldsymbol{V}''\theta''}]$ denotes the effects on the mean flow from the eddy transport of heat (ETH); $-\nabla \cdot [(\overline{p} - p_{\mathrm{R}})\langle\boldsymbol{V}\rangle]$ is the work of the mean pressure (WMP); $C(\overline{\rho}e_{\mathrm{m}}, \overline{\rho e_{\mathrm{t}}})$ represents the conversion between e_{m} and e_{t} (CEMT); $G(\overline{\rho}e_{\mathrm{m}})$ is the generation of e_{m} (GEM) due to diabatic processes; $-\nabla \cdot (\overline{\rho\boldsymbol{V}k_{\mathrm{t}}})$ stands for the transport of k_{t} (TKT); $-\nabla \cdot (\overline{\boldsymbol{F} \cdot \boldsymbol{V}''})$ represents the molecular stress effect on the eddy flow (MSE); $C(\overline{\rho k_{\mathrm{t}}}, \overline{\rho e_{\mathrm{t}}})$ denotes the eddy flow's baroclinic energy conversion (BCE); $D(\overline{\rho k_{\mathrm{t}}})$ is the molecular dissipation of k_{t} (MDE); $-\nabla \cdot (\overline{\rho\boldsymbol{V}e_{\mathrm{t}}})$ represents the transport of e_{t} (TET); $-\nabla(\overline{p'\boldsymbol{V}''})$ denotes the work from the perturbation pressure (WPP); and $G(\overline{\rho e_{\mathrm{t}}})$ is the generation of e_{t} (GET) owing to diabatic processes. In addition, for each of the budget equations, Eqs. (1)–(4), the sum of all the right-hand side terms, except for the friction-related terms, is defined as its total (TOT) term. Abbreviations of the equations are shown in Table 1.
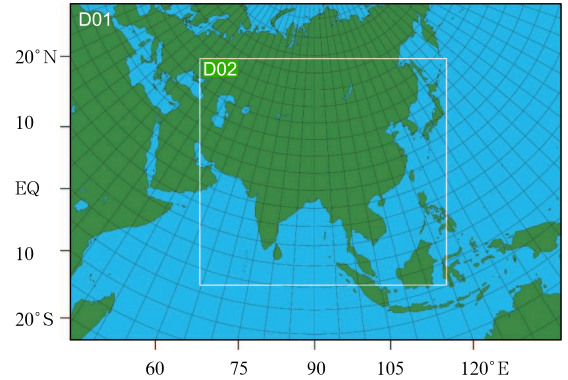

Fig. 1. The two domains used for the simulation in this study.

Table 1. Abbreviations and their original terminology

Abbreviation	Original terminology	Abbreviation	Original terminology
k_m	Mean kinetic energy	ETH	Effects of eddy transport of heat
k_t	Perturbation kinetic energy	WMP	Work of the mean pressure
e_m	Mean exergy	CEMT	Conversion between e_m and e_t
e_t	Perturbation exergy	GEM	Generation of e_m due to diabatic processes
MTKM	Mean transport of k_m	TKT	Transport of k_t by the mean and eddy flows
RSW	Reynolds stress work on the mean flow	MSE	Molecular stress effect on the eddy flow
MSM	Molecular stress effect on the mean flow	BCE	Baroclinic energy conversion (eddy flow)
CKMT	Conversion between k_m and k_t	MDE	Molecular dissipation of k_t
BCM	Baroclinic energy conversion (mean flow)	TET	Transport of e_t by the mean and eddy flows
MDM	Molecular dissipation of k_m	WPP	Work of the perturbation pressure
MTEM	Mean transport of e_m	GET	Generation of e_t due to diabatic processes

3. Overview of the PHRE and validation of the simulation

Recently, based on a 752-station daily precipitation observation dataset, Wang et al. (2014) conducted a statistical and classification analysis on the PHREs over South China during 1981–2011. They classified these events that occurred over the Yangtze and Huaihe River valley into three basic patterns, i.e., south-box pattern (to the south of the Yangtze River), north-box pattern (to the north of the Yangtze River), and along the Yangtze River pattern. In this study, a typical south-box pattern PHRE, which persisted for around 9 days (from 0000 UTC 17 to 0000 UTC 26 June 2010) and induced a maximum 9-day accumulated precipitation of greater than 600 mm (Fig. 2), was selected for detailed analysis.

During this 2010 PHRE case, a 500-hPa short-wave trough maintained quasi-stationary over the middle and lower reaches of the Yangtze River (Fig. 3a). The south box was located ahead of the trough base, where there was warm temperature advection and cyclonic-vorticity advection (Fig. 3b). Quasi-geostrophic forcings associated with the warm temperature advection and cyclonic-vorticity advection were conducive to a lowering of low-level pressure and maintenance of ascending motion—both of which favored the sustainment of precipitation. In addition, the south box was also located on the right side of the entrance region of the 200-hPa jet, where the jet-related secondary circulation prompted lower-level convergence and ascending motion—both of which were conducive to the PHRE's persistence. From Fig.

3b, it can be seen that a closed high center maintained at around 35°N, 115°E during this case, to the south of which easterly wind appeared. The easterly wind met the southwesterly wind within the south box, which formed a significant horizontal shear line directly triggering the PHRE. The southwesterly wind within the south box reached the criterion of a lower-jet (12 m s^{-1}), which brought abundant moisture inside. Correspondingly, strong moisture flux convergence appeared and persisted within the south box, which provided the necessary moisture conditions. Corresponding to the orientation of the aforementioned lower-level shear line, the accumulated precipitation mainly stretched zonally, with its center around 28°N, 118°E, where there was a strong moisture convergence center (Fig. 3b).

In this study, the simulation reproduced the 500-hPa shortwave trough and the 850-hPa shear line reasonably well (figure omitted), including their locations, intensity, orientation, and variations. Comparisons between Figs. 2a and 2b show that the simulation reproduced the zonally stretching rainband reasonably well, and the simulated maximum precipitation center was also located at around 28°N, 118°E, and was of an intensity greater than 600 mm. Although the simulation overestimated the precipitation to the southwest of the south box and around the western part of Jiangxi Province, generally, the intensity and fundamental pattern of the simulation were consistent with the observation. Moreover, from Fig. 2c, it can be seen that the south-box averaged 6-h accumulated precipitation was very similar in the simulation and observation, including the variation, intensity, and
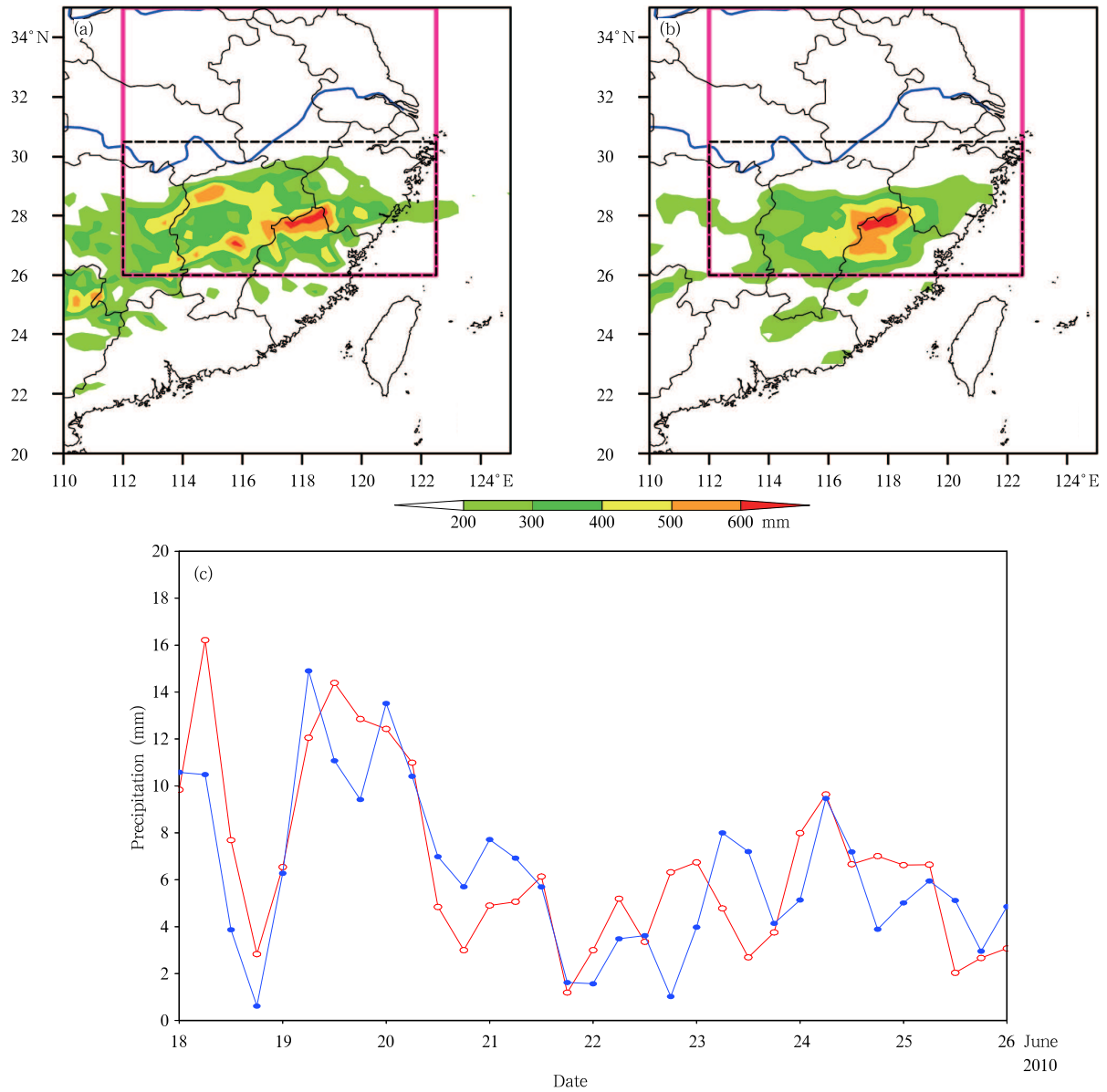
Fig. 2. (a) Simulated 9-day (0000 UTC 17 to 0000 UTC 26 June 2010) accumulated precipitation (color-shaded; mm) and (b) corresponding observed accumulated precipitation (red box marks the key region for precipitation; black dashed line divides the region equally into the north and south box). (c) The 6-h simulated south-box averaged precipitation (blue line) and the 6-h south-box averaged observed precipitation (red line; mm).

occurrence time of maximum precipitation. As mentioned above, although there were inevitable differences between the simulation and observation (Figs. 2 and 3), the overall simulation reproduced the primary features of the observation reasonably well, and thus it was deemed that the simulation could be used for further analysis.

4. Energy budget results

Figure 4a shows the 9-day averaged k_t at 1.5 km, from which it can be seen that the rainband was well consistent with the strong k_t zone. This intense k_t zone was associated with the lower-level horizontal shear line (Fig. 3b), which was the direct trigger for
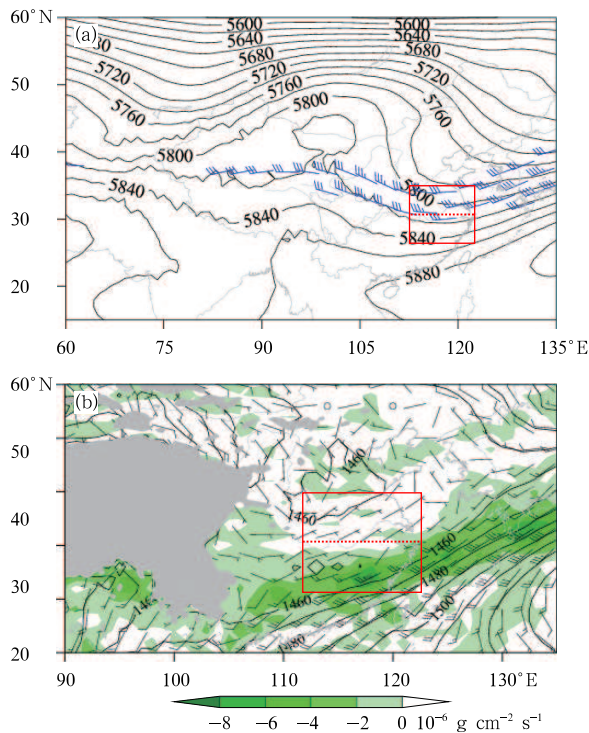
Fig. 3. (a) The simulated 9-day (0000 UTC 17 to 0000 UTC 26 June 2010) averaged 500-hPa geopotential height (gpm) and 200-hPa wind above 30 m s^{-1} (full bar represents 10 m s^{-1}). (b) The simulated 9-day averaged 850-hPa wind (full bar represents 5 m s^{-1}) and the entire air column moisture flux divergence (color-shaded; 10^{-6} g cm^{-2} s^{-1}). The red box marks the key region for precipitation, and the dashed line divides the region equally into the north and south boxes.

this 2010 PHRE case. Therefore, from the viewpoint of energy, mechanisms accounting for the persistence of this strong k_t zone were the primary reason for this PHRE case. Figure 4b shows that except for the strong k_t zone, the south box also has strong e_t, implying that the baroclinicity was strong during the PHRE. In contrast, the north box had weak k_t and e_t, and this can explain why the precipitation was weak. From Fig. 5c, it is seen that the south-box averaged k_t is very similar in terms of its variation to that of precipitation. This further confirms that the lower-level eddy flows were the direct triggers for this 2010 PHRE case, and the energy budget can effectively demonstrate how the precipitation sustained

for a period of nearly 9 days. For other energies, during the PHRE, k_m reached its maximum in the upper troposphere, corresponding to the upper-level jet (Figs. 5a and 6a); whereas in the middle troposphere, it had minimum values (Fig. 6a). The maximum zones of both e_m and e_t appeared in the lower troposphere (Figs. 5b, 5d, 6b, and 6d), whereas the middle troposphere generally featured minimum baroclinicity. It should be noted that the lower-level strong baroclinicity provided highly favorable energy conditions for the maintenance of precipitation through the release of exergy (available potential energy).

As illustrated in Fig. 7a, for the whole period of this PHRE case, the south-box averaged k_t generally featured TOT-k_t > 0 below 2.5 km, which means that the eddy flows' KE maintained intensity in the lower-level troposphere. This explains why the precipitation lasted for a long period. For other energies, the TOT-e_t was negative at lower levels, which implies that the eddy flows' baroclinicity was generally weakening. Overall, the mean flows' KE and baroclinicity showed a decreasing trend (TOT-k_m < 0) and an increasing trend (TOT-e_m > 0), respectively. The baroclinic energy conversion from k_m to e_m can account for a proportion of the opposite trends of k_m and e_m (Fig. 7b).

From Fig. 8c, it can be seen that the eddy flows' KE had opposite trends in the lower troposphere and the middle to upper troposphere (it should be noted that the friction-related effects were not considered). The baroclinic energy conversion from e_t to k_t (BCE > 0) dominated the positive trend of the lower-level eddy flows' KE (Fig. 8d); and in the middle troposphere, the baroclinic energy conversion was also the most important factor accounting for the negative trend of k_t (the conversion was from k_t to e_t). From Fig. 8e, it can be seen that, in the lower troposphere, the eddy transport of k_t was mainly transporting energy out of the south box (except for the period of 19–20 June), which made the south box an energy source of k_t. Below 3 km, the term CKMT generally remained positive (Figs. 7b and 8b). This means that a downscaled energy cascade of KE appeared, which transferred energy from the mean flow
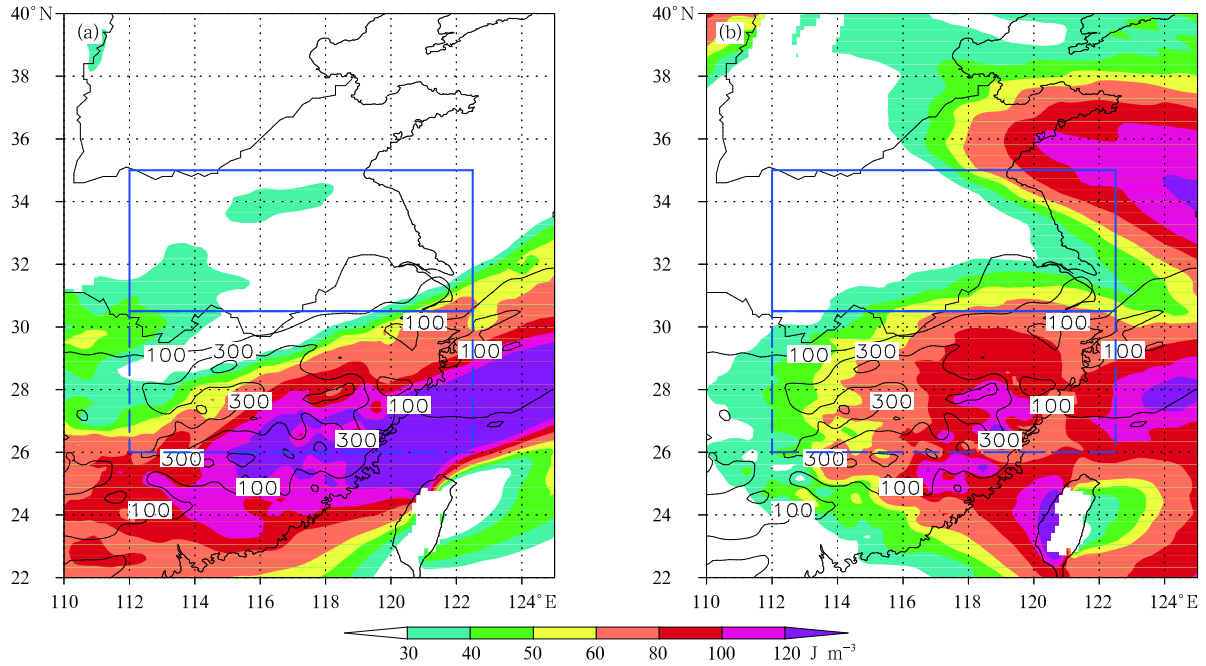
Fig. 4. The 9-day simulated accumulated precipitation (black contours; mm) and the 9-day simulated averaged (a) perturbation kinetic energy (color-shaded; J m^{-3}) and (b) perturbation exergy (color-shaded; J m^{-3}) at the height of 1.5 km. The blue box marks the key region for precipitation, divided equally into the north box (solid) and south box (dashed).
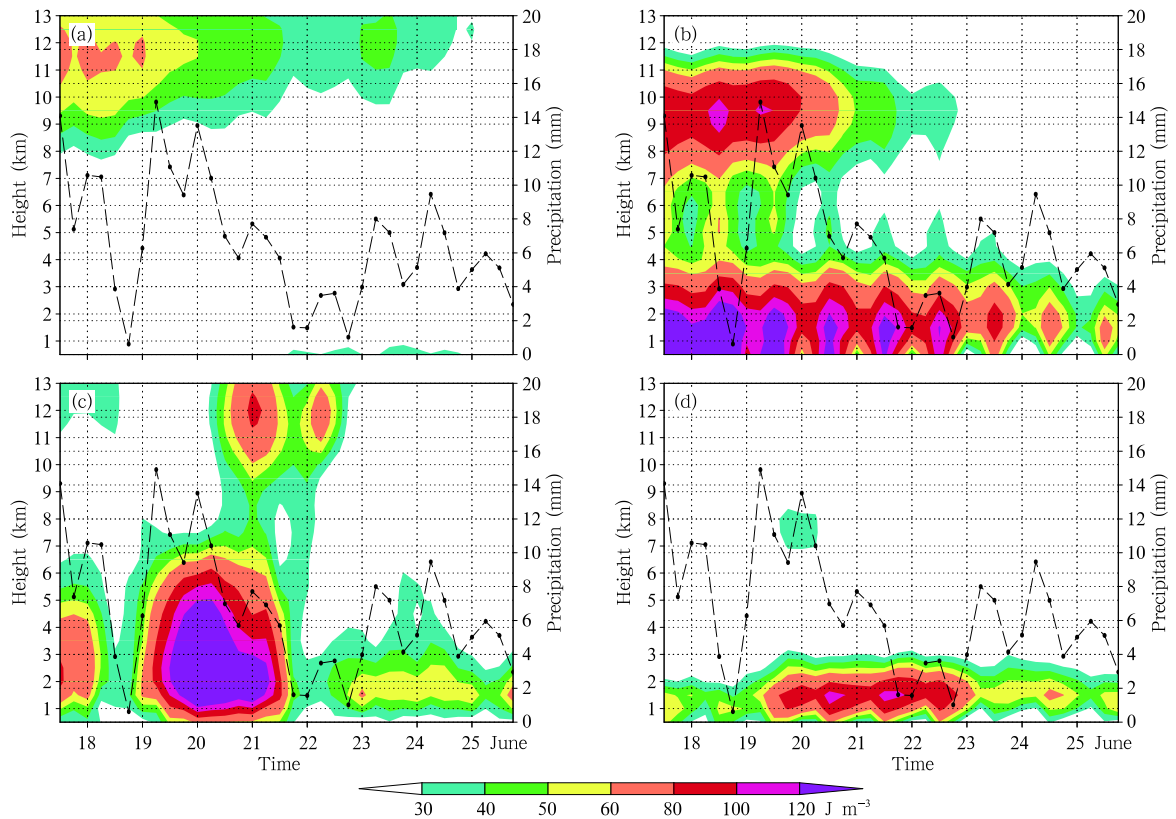

Fig. 5. The south-box averaged energy (color-shaded; J m^{-3}) and 6-h simulated accumulated precipitation (black dashed line; mm). (a) Mean kinetic energy, (b) mean exergy, (c) perturbation kinetic energy, and (d) perturbation exergy.
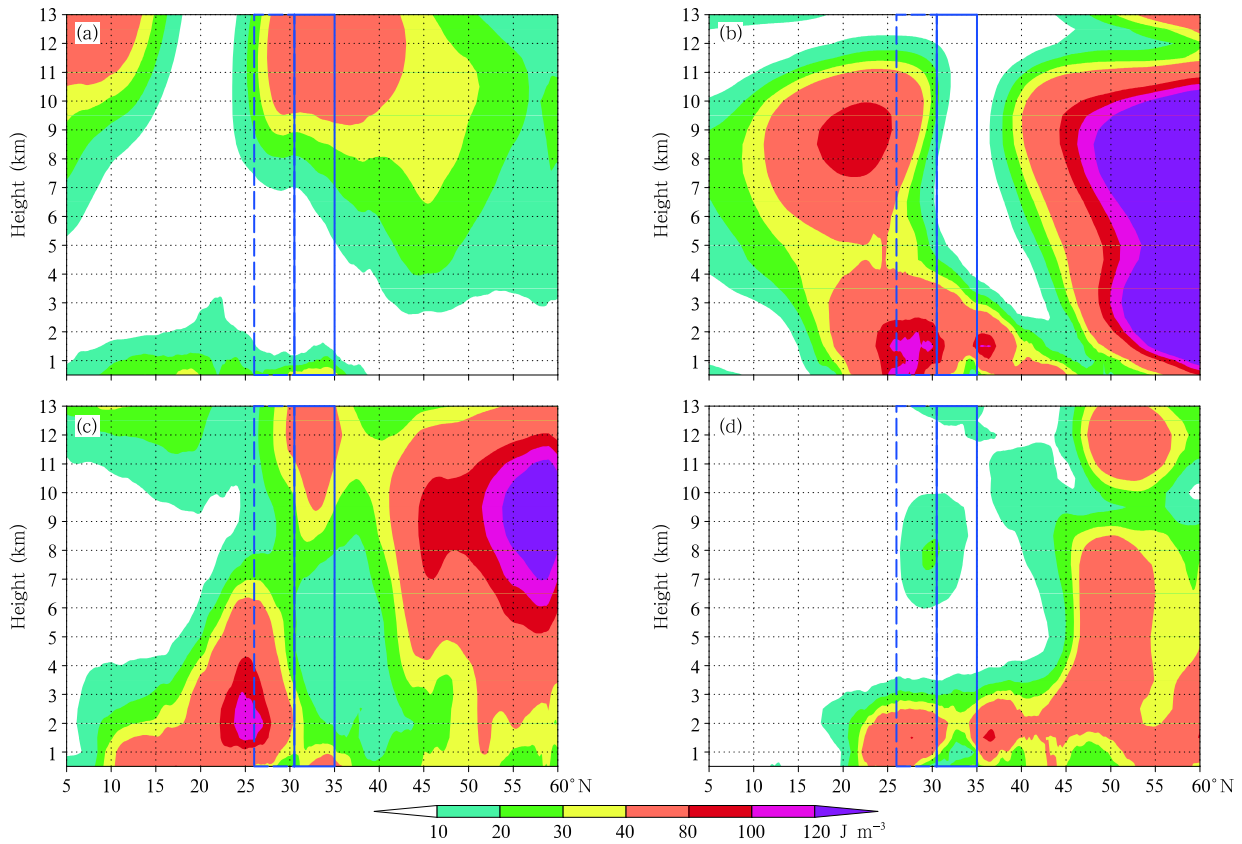
Fig. 6. The 9-day averaged zonal mean energy (color-shaded; J m^{-3}). The blue box marks the key region for precipitation, divided equally into the north box (solid) and south box (dashed). (a) Mean kinetic energy, (b) mean exergy, (c) perturbation kinetic energy, and (d) perturbation exergy.
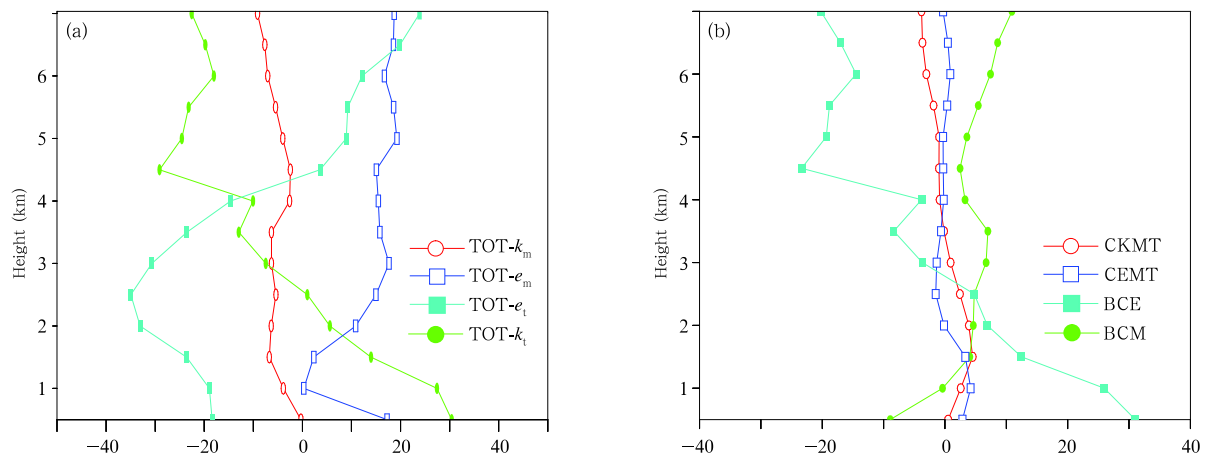

Fig. 7. The 9-day averaged south-box mean (a) TOT (10^{-4} W m^{-3}) and (b) budget (10^{-4} W m^{-3}) terms.

to the eddy flow, and thus favored the maintenance of k_t in the lower troposphere directly.

As Fig. 9d shows, the main trend of the south-box

averaged e_t generally had an opposite pattern compared to the trend of k_t (Fig. 8c): in the lower troposphere, a significant negative trend was maintained,

whereas a positive trend primarily dominated the middle to upper levels. At the lower levels, e_t decreased mainly due to the baroclinic energy conversion from e_t to k_t (Fig. 9g); while in the middle to upper troposphere, the diabatic processes dominated the production of e_t (Fig. 9c). In the lower troposphere, the perturbation pressure (term WPP) mainly favored the e_t production below 2 km, whereas it worked conversely at the upper levels (Fig. 9b). The diabatic processes mainly reduced the lower-level e_t (Fig. 9c) via evapo-

rative cooling effects. The eddy transport of e_t was primarily divergent within the south box before 21 June (Fig. 9f), which reduced e_t; and then it changed to being convergent later on, which served as an energy sink. The term CEMT was mainly positive at lower levels (Fig. 9e), meaning that a downscaled energy cascade of energy occurred. This process transferred energy from the mean flows' e_m to the eddy flows' e_t, which favored the sustainment of the eddy flows' baroclinicity. It should be noted that this downscaled en-
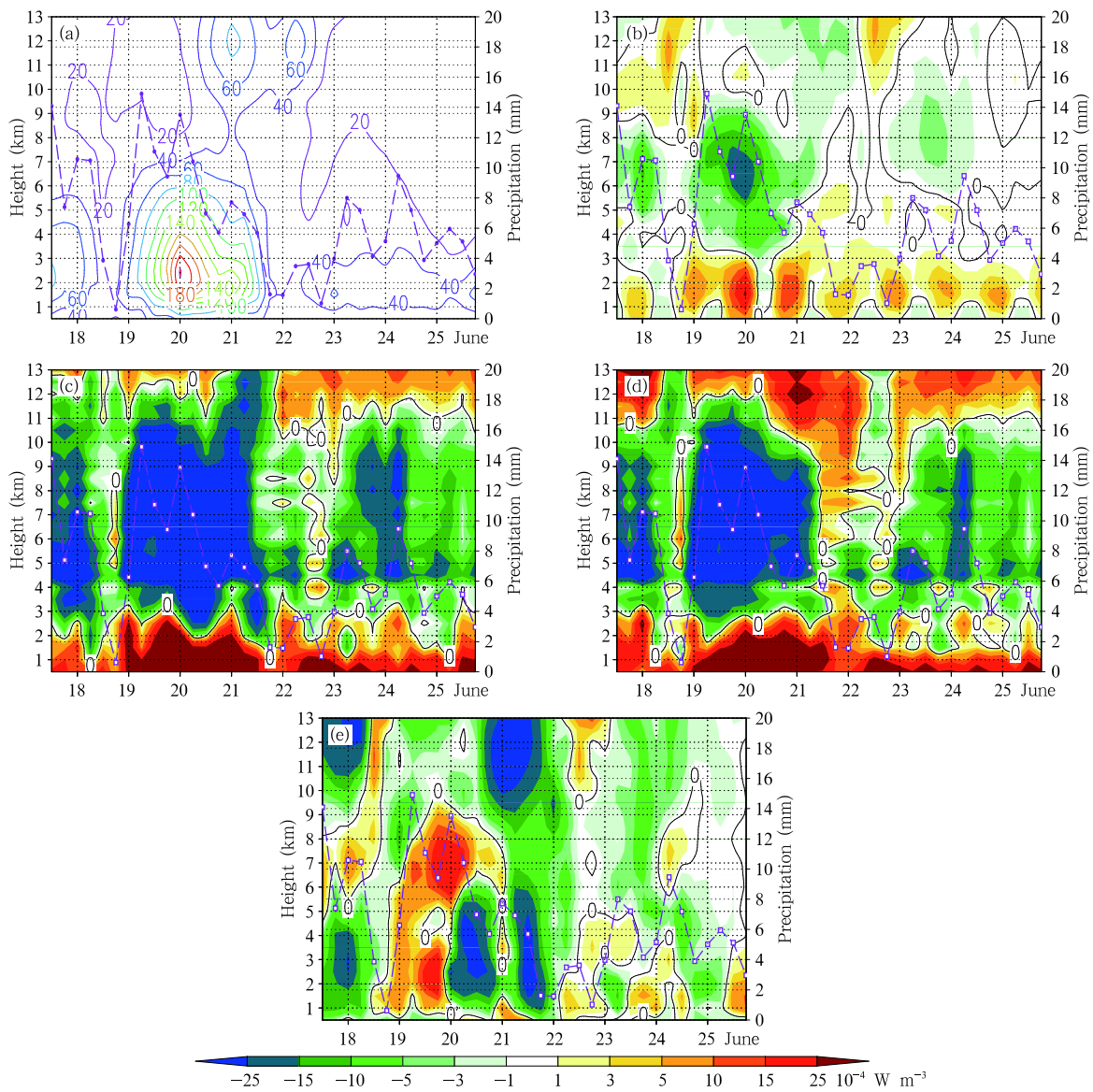

Fig. 8. The south-box averaged (a) k_t (contours; J m^{-3}) and its budget terms (color-shaded: 10^{-4} W m^{-3}) (b) CKMT, (c) TKT + CKMT + BCE, (d) BCE, and (e) TKT. The purple dashed line shows the variation of the south-box averaged 6-h precipitation (mm).
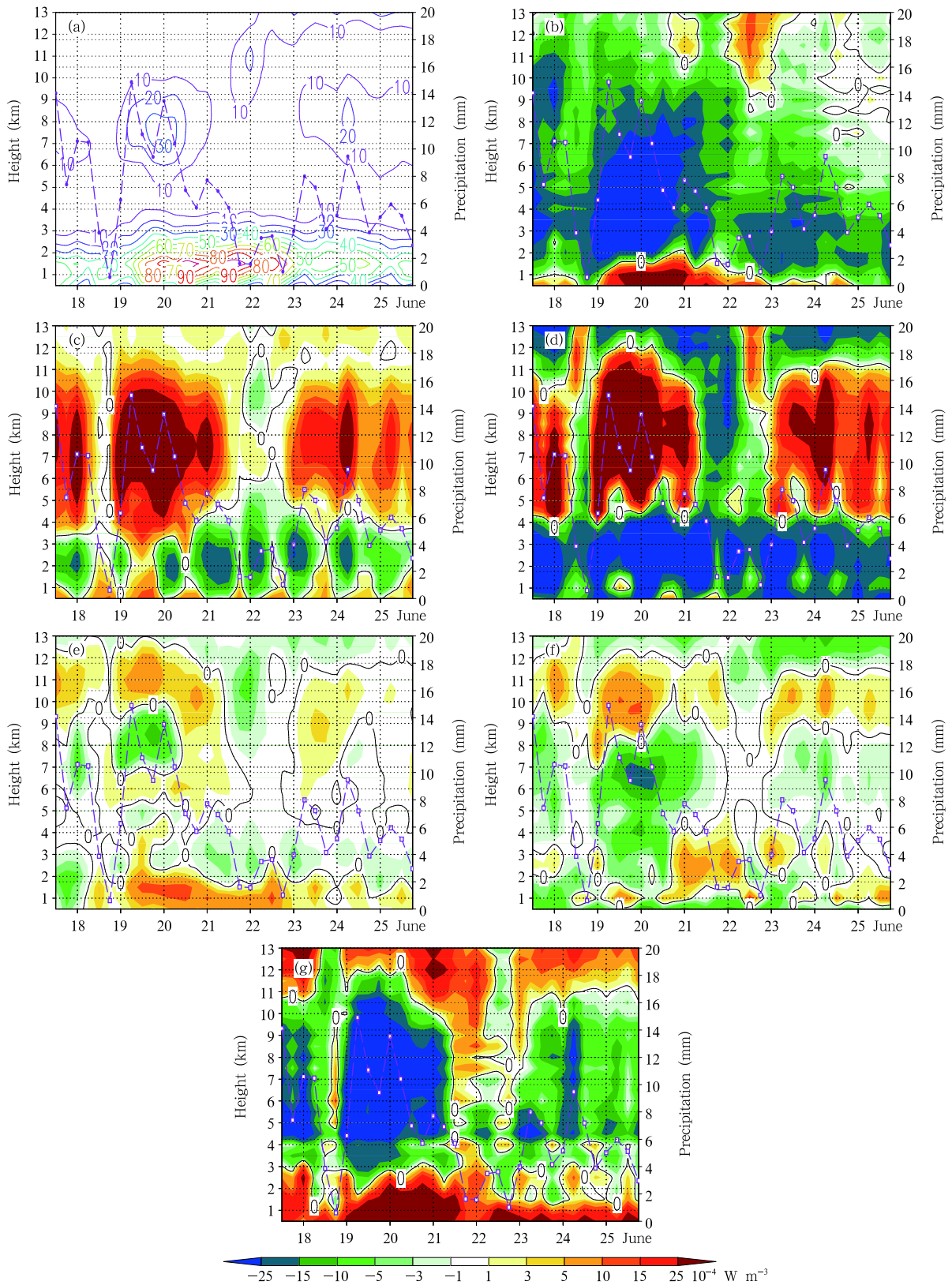
Fig. 9. As in Fig. 8, but for e_t and its budget terms. (a) e_t, (b) WPP, (c) GET, (d) TET+WPP+CEMT−BCE+GET, (e) CEMT, (f) TET, and (g) BCE.

ergy cascade process may have favored the mainte-
nance of the precipitation-related eddy flows indi-
rectly, through the baroclinic energy conversion.

   For the mean flows' KE, this generally showed a
weakening trend (Figs. 7a and 10c). In the upper
troposphere, this weakening mainly corresponded to
the deceleration of the upper-level jet (Fig. 3a), while
in the lower troposphere it was primarily related to

the weakening of the low-pressure zone (figure omit-
ted). The baroclinic energy conversion from $k_{\rm m}$ to $e_{\rm m}$
was the main reason for the negative trend of $k_{\rm m}$ (Fig.
10f). The term CKMT showed different effects on the
mean flows' KE at different layers (Fig. 10d): in the
middle to upper troposphere, it mainly corresponded
to an upscaled energy cascade process (CKMT < 0),
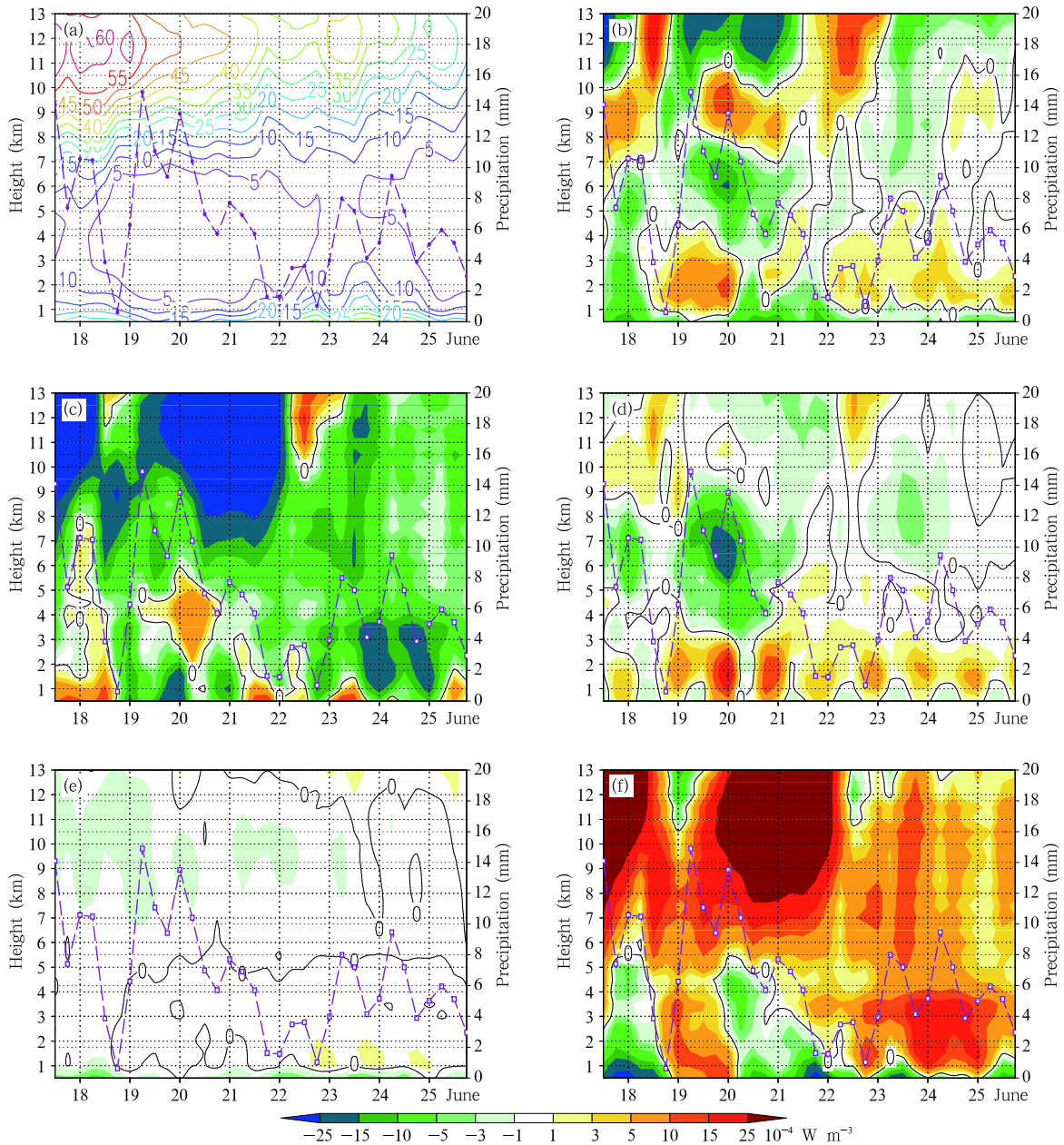during which energy was transferred from the eddy

Fig. 10. As in Fig. 8, but for $k_{\rm m}$ and its budget terms. (a) $k_{\rm m}$, (b) RSW, (c) MTKM+RSW-CKT-BCM, (d) CKMT,
(e) MTKM, and (f) BCM.

flow to the mean flow. However, the intensity of this upscaled energy cascade of KE was weaker than the intensity of the baroclinic energy conversion (Fig. 10f). In the lower troposphere, a downscaled energy cascade process of KE occurred (CKMT > 0), and this term was a dominant factor for the weakening trend of the lower-level k_m (Figs. 10d and 10f). The transport of k_m by the mean flow generally triggered divergence within the south box (Fig. 10e), which was also detrimental for the sustainment of k_m. The Reynolds stress work (term RSW) was mainly favorable for the maintenance of k_m in the lower troposphere (Fig. 10b); whereas in the middle to upper troposphere, its effects changed with time (in a positive–negative–positive–negative–positive pattern).

The conditions were generally favorable for the maintenance of the baroclinicity of the mean flow (e_m) in the lower troposphere (Figs. 7a and 11d). This lower-level trend was mainly dominated by the baroclinic energy conversion from k_m to e_m (Fig. 11c), the diabatic processes (Fig. 11f), and the work of the mean pressure (Fig. 11e). It should be noted that the effects associated with the eddy transport of heat (term ETH) mainly favored the sustainment of lower-level e_m before 21 June, and worked conversely later (Fig. 11b). In addition, terms MTEM and CEMT primarily reduced the lower-level e_m through transporting energy out of the south box (Fig. 11g) and causing a downscaled energy cascade process of energy (Fig. 11h), respectively.

5. Conclusions and discussion

In this study, a PHRE case (with maximum accumulated precipitation greater than 600 mm appearing over the Yangtze River valley) that lasted from 0000 UTC 17 to 0000 UTC 26 June 2010, was reasonably reproduced by the WRF model. By using a set of energy budget equations (Eqs. (1)–(4)) that divided the real meteorological field into the mean flow and the eddy flow (precipitation triggers), the interactions sustaining the PHRE were analyzed.

During the 2010 PHRE case, the precipitation-related eddy flows interacted with their BCs intensely.

A long-lived quasi-stationary lower-level shear line ahead of the 500-hPa shortwave trough was the direct trigger for this rainfall event (Fig. 3). Strong perturbation KE was associated with the shear line, and it showed a similar variation to that of the precipitation (Fig. 8a). The energy budget results in Fig. 12 demonstrated that, in the lower troposphere, perturbation KE was sustained mainly through the baroclinic energy conversion associated with convection activities (term BCE). Alongside this, the downscaled energy cascade processes of KE were also favorable. Similarly, a downscaled energy cascade of exergy also appeared in the lower troposphere. This downscaled energy cascade favored the precipitation-related eddy flow indirectly, via the baroclinic energy conversion from e_t to k_t. These downscaled energy cascade processes reflect the direct influences of the mean flow on the precipitation-related eddy flow. Meanwhile, a baroclinic energy conversion occurred in the mean flow, which reduced k_m, and the downscaled energy cascade of KE also enhanced this weakening. It should be noted that similar results were also found by Fu et al. (2013), during which the lower-level baroclinic energy conversion sustained two heavily precipitative mesoscale vortices. Moreover, a recent study of a long-lived mesoscale vortex that induced a PHRE over the Yangtze River basin (Fu et al., 2015) also confirmed the importance of the lower-level downscaled energy cascade of KE in sustaining the precipitation.

In the middle troposphere, very different energy cycles appeared compared to those in the lower troposphere (Fig. 12). The upscaled energy cascade processes appeared in both the KE and exergy. This can represent the reactionary effects of the precipitation-related eddy flows on their BCs. Overall, the reactionary effects in the thermodynamical field were weak (still cannot be ignored) with respect to the mean flow's variation (considering exergy); whereas in the dynamical field, the effects were important for the mean flow's variation (considering KE). Similar to that in the lower troposphere, a baroclinic energy conversion from k_m to e_m also appeared in the middle troposphere. Moreover, different from that in the lower troposphere, a baroclinic conversion from k_t to e_t,
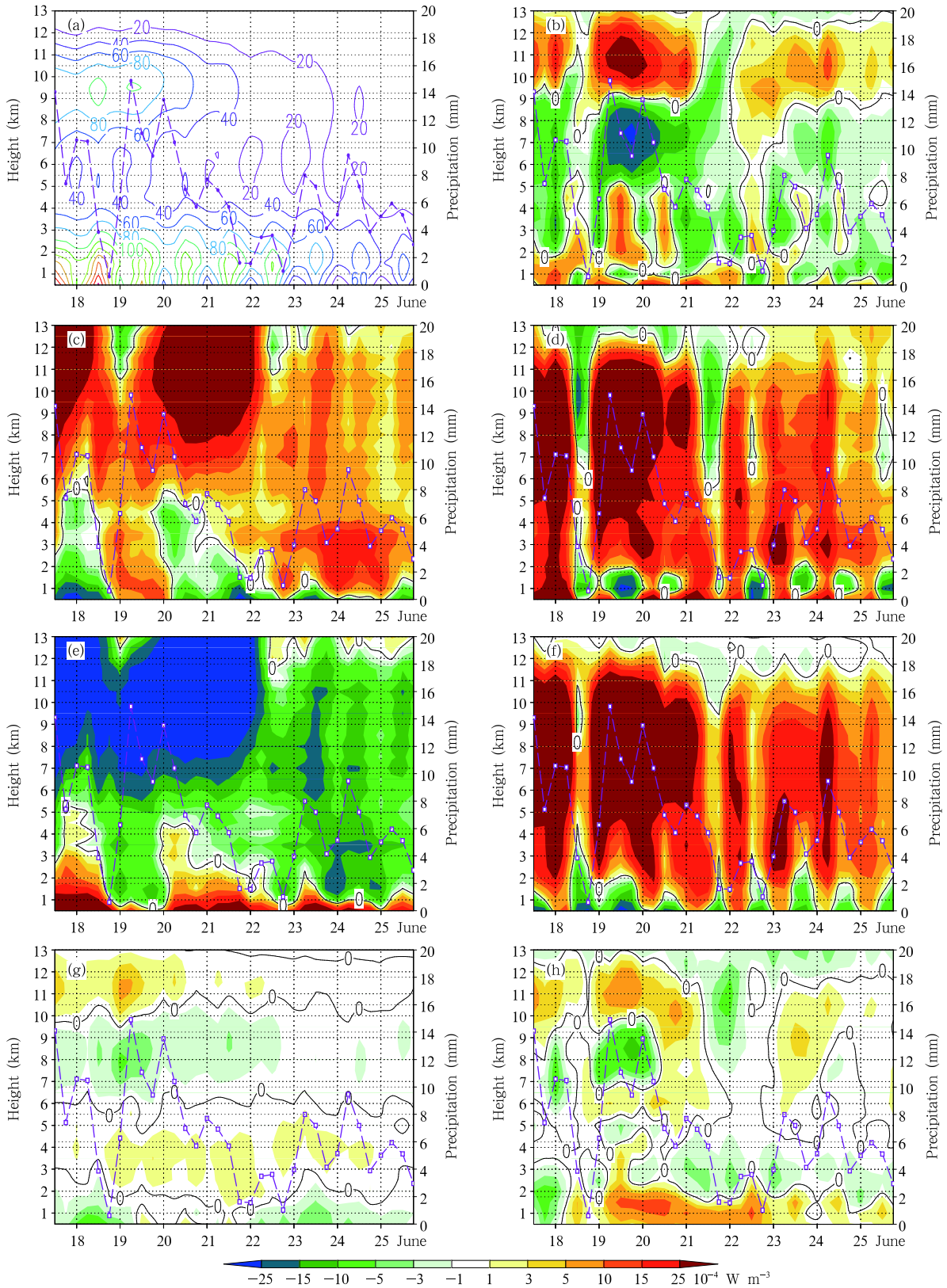
Fig. 11. As in Fig. 8, but for e_m and its budget terms. (a) e_m, (b) ETH, (c) BCM, (d) MTEM+ETH+WMP-CEMT+BCM+GEM, (e) WMP, (f) GEM, (g) MTEM, and (h) CEMT.

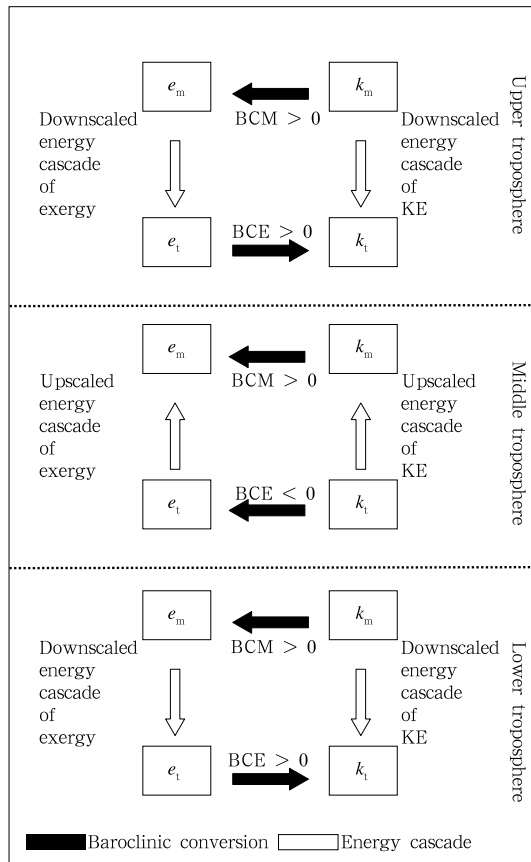　　　　　　　　JOURNAL OF METEOROLOGICAL RESEARCH　　　　　　　　VOL.30

Fig. 12. Schematic illustration of the dominant factors governing the energy cycles in different layers during the 2010 PHRE case.

which reduced the intensity of eddy flow, occurred in the middle troposphere.

　　In the upper troposphere, very similar energy cycles to those in the lower troposphere appeared (Fig. 12). The weakening of the mean flows' KE mainly corresponded to the deceleration of the upper-level jet. The baroclinic energy from e_m to k_m dominated this process, and the downscaled energy cascade of KE also enhanced this weakening. Overall, in this layer, conditions were also favorable for the persistence of eddy flows.

REFERENCES

Chen, F., and J. Dudhia, 2001: Coupling an advanced land surface-hydrology model with the Penn State-NCAR MM5 modeling system. Part I: Model implementation and sensitivity. *Mon. Wea. Rev.*, **129**, 569–585.

Chen Hong and Zhao Sixiong, 2004: Heavy rainfalls in South China and related circulation during HUAMEX period. *Chinese J. Atmos. Sci.*, **28**, 32–47. (in Chinese)

Chen, G. T. J., C. C. Wang, and L. F. Lin, 2006: A diagnostic study of a retreating Meiyu front and the accompanying low-level jet formation and intensification. *Mon. Wea. Rev.*, **134**, 874–896.

Cho, H. R., and G. T. J. Chen, 1995: Meiyu frontogenesis. *J. Atmos. Sci.*, **52**, 2109–2120.

Ding Yihui, 1994: Some aspects of rainstorm and mesoscale meteorology. *Acta Meteor. Sinica*, **52**, 274–284. (in Chinese)

Ding Yihui, Liu Junjie, Sun Ying, et al., 2007: A study of the synoptic-climatology of the Meiyu system in East Asia. *Chinese J. Atmos. Sci.*, **31**, 1082–1101. (in Chinese)

Fu Shenming, Zhao Sixiong, Sun Jianhua, et al., 2010: One kind of vortex causing heavy rainfall during pre-rainy season in South China. *Chinese J. Atmos. Sci.*, **34**, 235–252. (in Chinese)

Fu, S.-M., W.-L. Li, J.-H. Sun, et al., 2011: A budget analysis of a long-lived tropical mesoscale vortex over Hainan in October 2010. *Meteor. Atmos. Phys.*, **114**, 51–65.

Fu Shenming, Yu Fei, Wang Donghai, et al., 2013: A comparison of two kinds of eastward-moving mesoscale vortices during the Meiyu period of 2010. *Sci. China (Ser. D)*, **56**, 282–300.

Fu, S.-M., W.-L. Li, and J. Ling, 2015: On the evolution of a long-lived mesoscale vortex over the Yangtze River basin: Geometric features and interactions among systems of different scales. *J. Geophys. Res.*, **120**, 11889–11917, doi: 10.1002/2015JD023700.

Fu, S.-M., D.-S. Li, J.-H. Sun, et al., 2016: A 31-year trend of the hourly precipitation over South China and the underlying mechanisms. *Atmos. Sci. Lett.*, **17**, 216–222, doi: 10.1002/asl.645.

Hong, S.-Y., Y. Noh, and J. Dudhia, 2006: A new vertical diffusion package with an explicit treatment of entrainment processes. *Mon. Wea. Rev.*, **134**, 2318–2341.

Hou Jun and Guan Zhaoyong, 2013: Climatological characteristics of frontogenesis and related circulations over East China in June and July. *Acta Meteor. Sinica*, **27**, 144–169, doi: 10.1007/s13351-013-0202-z.

Kain, J. S., 2004: The Kain–Fritsch convective param-
eterization: An update. *J. Appl. Meteor.*, **43**,
170–181.

Kucharski, F., and A. J. Thorpe, 2000: Local energetics
of an idealized baroclinic wave using extended ex-
ergy. *J. Atmos. Sci.* **57**, 3272–3284.

Li, D.-S., J.-H. Sun, S.-M. Fu, et al., 2016: Spatiotem-
poral characteristics of hourly precipitation over
central eastern China during the warm season of
1982–2012. *Int. J. Climatol.*, **36**, 3148–3160, doi:
10.1002/joc.4543.

Lim, K.-S. S., and S.-Y. Hong, 2010: Development of an
effective double-moment cloud microphysics scheme
with prognostic cloud condensation nuclei (CCN)
for weather and climate models. *Mon. Wea. Rev.*,
138, 1587–1612.

Michalakes, J., J. Dudhia, D. Gill, et al., 2004: The
Weather Research and Forecast Model: Software ar-
chitecture and performance. Proceedings of the 11th
ECMWF Workshop on the Use of High Performance
Computing in Meteorology, Boulder, Colorado, 25–
29 October, Mesoscale and Microscale Meteorology
Division, National Center for Atmospheric Research,
299 pp.

Ninomiya, K., and H. Muraki, 1986: Large-scale circula-
tions over East Asia during Baiu period of 1979. *J.
Meteor. Soc. Japan*, **64**, 409–429.

Reynolds, R. W., T. M. Smith, C. Y. Liu, et al., 2007:
Daily high-resolution-blended analyses for sea sur-
face temperature. *J. Climate*, **20**, 5473–5496.

Tao Shiyan and Xu Shuying, 1962: Some aspects of
the circulation during the periods of the persistent
drought and flood in Yangtze and Hwai-ho valleys
in summer. *Acta Meteor. Sinica*, **32**, 1–10. (in
Chinese)

Tao Shiyan, 1980: *Rainstorms in China*. Science Press,
Beijing, 225 pp. (in Chinese)

Wang Huijie, Sun Jianhua, Wei Jie, et al., 2014: Clas-
sification of persistent heavy rainfall events over
southern China during recent 30 years. *Climatic

Environ. Res.*, **19**, 713–725. (in Chinese)

Xia Rudi, Zhao Sixiong, and Sun Jianhua, 2006: A study
of circumstances of meso-β-scale systems of strong
heavy rainfall in warm sector ahead of fronts in
South China. *Chinese J. Atmos. Sci.*, **30**, 988–
1008, doi: 10.3878/j.issn.1006-9895.2006.05.26. (in
Chinese)

Xia Rudi and Zhao Sixiong, 2009: Diagnosis and model-
ing of meso-β-scale systems of heavy rainfall in warm
sector ahead of front in South China (middle part
of Guangdong Province) in June 2005. *Chinese J.
Atmos. Sci.*, **33**, 468–488, doi: 10.3878/j.issn.1006-
9895.2009.03.06. (in Chinese)

Xu Guoqiang, Zhu Qiangen, and Ran Yufang, 2002:
Analyses of features and mechanisms of summer
monsoon onsets over SCS and its vicinity in 1998.
J. Appl. Meteor. Sci., **13**, 535–549. (in Chinese)

Yin, Z.-Y., Y. L. Cai, X. Y. Zhao, et al., 2009: An
analysis of the spatial pattern of summer persis-
tent moderate-to-heavy rainfall regime in Guizhou
Province of Southwest China and the control factors.
Theor. Appl. Climatol., **97**, 205–218.

Zhai, P. M., X. B. Zhang, H. Wan, et al., 2005: Trends
in total precipitation and frequency of daily pre-
cipitation extremes over China. *J. Climate*, **18**,
1096–1108.

Zhao Sixiong, Tao Zuyu, Sun Jianhua, et al., 2004: *Study
on Mechanism of Formation and Development of
Heavy Rainfalls on Meiyu Front in Yangtze River*.
China Meteorological Press, Beijing, 282 pp.

Zhao Sixiong and Fu Shenming, 2007: An analysis on
the southwest vortex and its environment fields dur-
ing heavy rainfall in eastern Sichuan Province and
Chongqing in September 2004. *Chinese J. Atmos.
Sci.*, **31**, 1059–1075. (in Chinese)

Zong Haifeng, C. Bueh, and Ji Liren, 2014: Wintertime
extreme precipitation event over southern China and
its typical circulation features. *Chin. Sci. Bull.*, **59**,
1036–1044.